ADVANCED FUNCTIONAL MATERIALS

Supporting Information

for *Adv. Funct. Mater.,* DOI: 10.1002/adfm.202300428

Resistive Switching and Current Conduction Mechanisms in Hexagonal Boron Nitride Threshold Memristors with Nickel Electrodes

Lukas Völkel, Dennis Braun, Melkamu Belete, Satender Kataria, Thorsten Wahlbrink, Ke Ran, Kevin Kistermann, Joachim Mayer, Stephan Menzel, Alwin Daus, and Max C. Lemme**

Supporting Information

Resistive Switching and Current Conduction Mechanisms in Hexagonal Boron Nitride Threshold Memristors with Nickel Electrodes

Lukas Völkel[1], Dennis Braun[1], Melkamu Belete[1], Satender Kataria[1], Thorsten Wahlbrink[2], Ke Ran[3,4], Kevin Kistermann[3], Joachim Mayer[3,4], Stephan Menzel[5], Alwin Daus[1], Max C. Lemme[1,2*]*

[1] Chair of Electronic Devices, RWTH Aachen University, Otto-Blumenthal-Str. 25, 52074 Aachen, Germany.

[2] AMO GmbH, Advanced Microelectronic Center Aachen, Otto-Blumenthal-Str. 25, 52074 Aachen, Germany.

[3] Central Facility for Electron Microscopy (GFE), RWTH Aachen University, Ahornstr. 55, 52074, Aachen, Germany.

[4] Ernst Ruska-Centre for Microscopy and Spectroscopy with Electrons (ER-C 2), Forschungszentrum Jülich, 52425, Jülich, Germany.

[5] Peter Gruenberg Institute (PGI-7), Forschungszentrum Juelich GmbH and JARA-FIT, 52425 Juelich, Germany.

Section S1: Schematic process flow

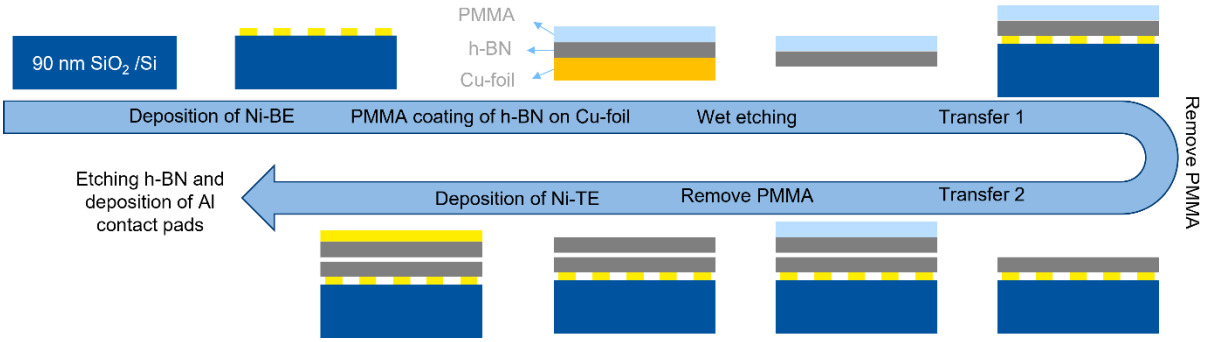

Figure S1: Schematic process flow. BE: Bottom electrode, TE: top electrode, Cu: copper, Al: aluminum, Ni: nickel.

Section S2: Current-voltage measurements on devices without h-BN

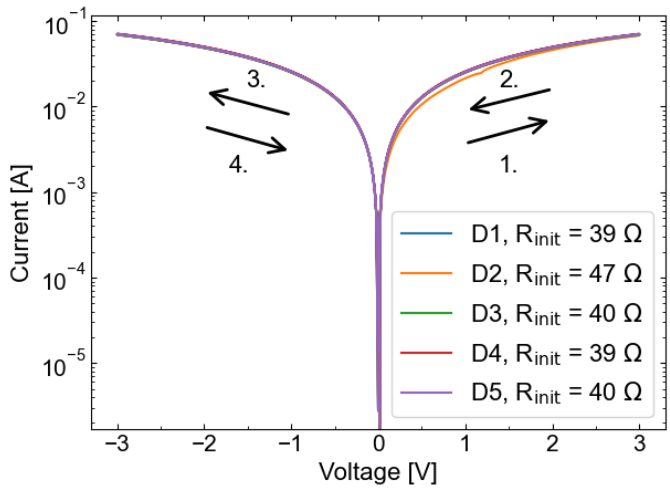

Figure S2**:** *I-V* curves measured of five different Ni/Ni memristors D1-D5.

To measure the possible influence of a nickel oxide layer between the Ni electrodes or between Ni and the Al contact pads on the RS behavior, we measure the initial resistance of devices without h-BN between the electrodes and subsequently apply a positive and a negative sweep with a maximum voltage of ±3 V. The initial resistance of all devices is only a few Ω and none of the devices show resistive switching. Thus, we can exclude an influence of the electrode material system on our resistive switching measurements.

Section S3: Histogram of h-BN E_{2g} peak position from Raman map spectra

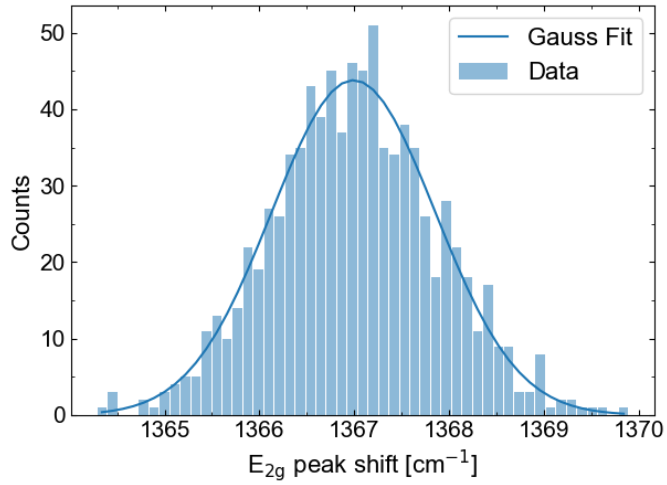

Figure S3: Histogram of extracted E_{2g}-peak position of all spectra in the Raman map. The peak positions are extracted by fitting a Lorentz-Peak to each Raman spectrum. A Gaussian distribution function with the center at 1367.0 cm^{-1} and a distribution width of σ = 0.9 cm^{-1} is fitted to the histogram data, which corresponds to 3-layer to bulk h-BN[1].

Section S4: HRTEM and van der Waals spacing

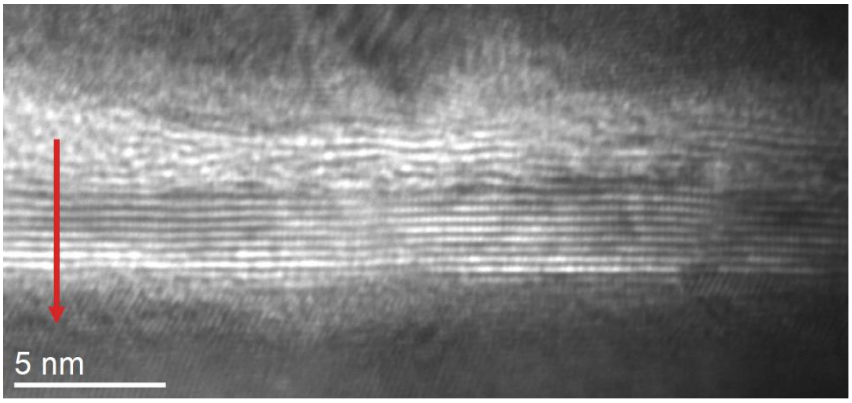

Figure S4-1: HRTEM image with the arrow indicating the position for line profile extraction.

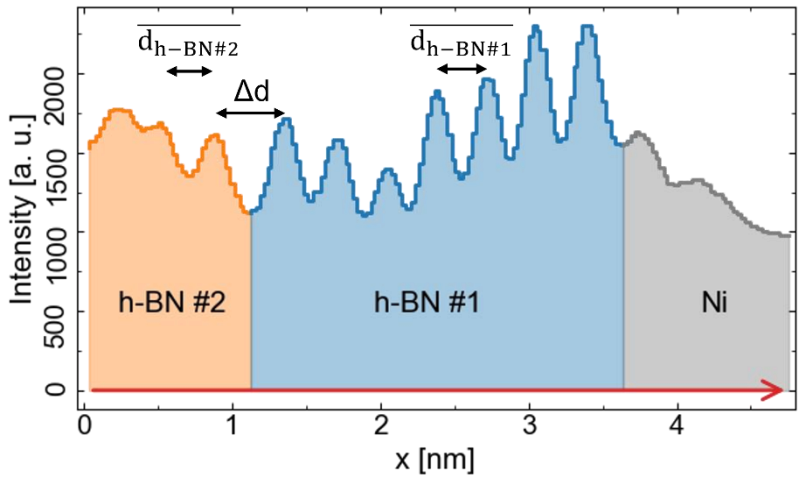

Figure S4-2: From HRTEM extracted line-profile. The orange, blue and gray regions are identified as h-BN film #2, h-BN film #1, and the Ni bottom electrode, respectively. $\overline{d_{h-BN\#1}}$ = 0.321 ± 0.029 nm is the mean interlayer distance of two adjacent h-BN layers in h-BN film 1, $\overline{d_{h-BN\#2}}$ = 0.340 ± 0.016 nm is the mean interlayer distance of two adjacent h-BN layers in film 2, and Δd = 0.479 nm is the spacing between h-BN film 1 and 2. The measured interlayer distance agrees with other literature values[2,3], whereas Δd is almost 30 % bigger.

Section S5: *I-V* Curves of endurance measurement

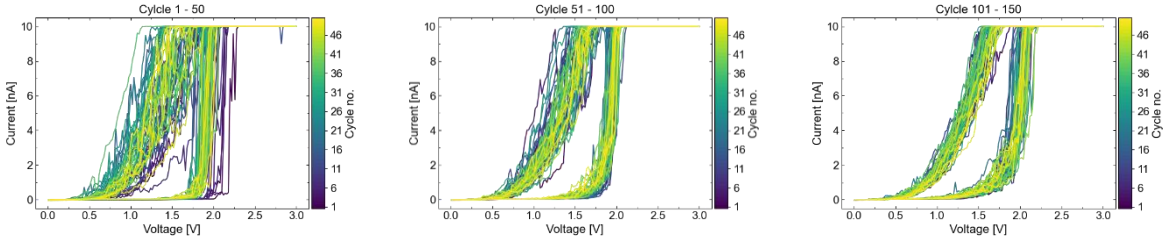

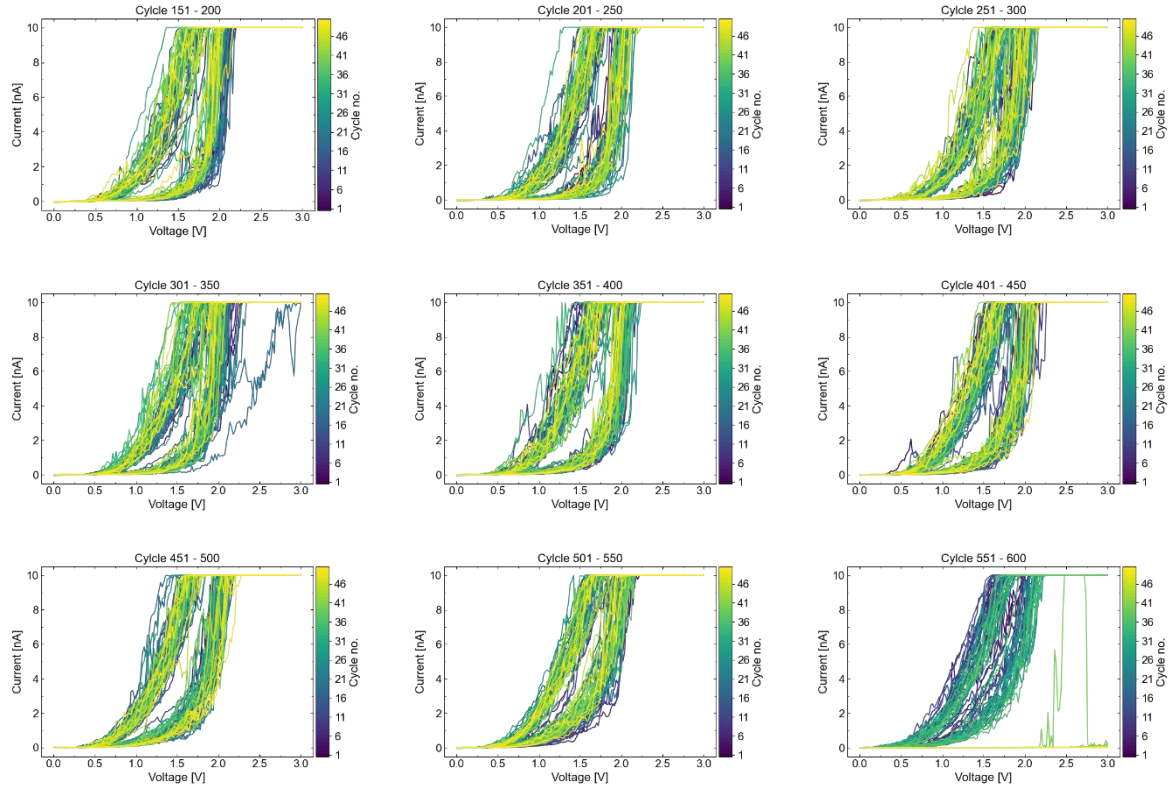

Figure S5: Complete set of *I-V* cycles measured during the endurance measurement. Every plot contains 50 cycles. The title of the plots denotes the respective cycle number range.

Section S6: Comparison of device performance with other literature

$I_{cc,max}/I_{cc,min}$ [A]	max. On/Off ratio	max. DC Endurance	Electrode material (BE/TE)	h-BN thickness	CMOS-compatible configuration	Reference
10^2	$5 \cdot 10^4$	5	Cu/Pt	3.5 nm	No (C-AFM)	[4]
10	$5 \cdot 10^5$	7	Pt/Ag	1.5 nm	No	[5]
5	$5 \cdot 10^7$	-	Ag/Pt, Ag/Ag	0.33 nm	No, No	[6]
10^2	10^4	2	Ti/Cu	5-7/15-20 layers	Yes	[7]
0	10^5	4	Fe/Ag	~ 15 layers	No	[8]
0	10^3	-	Fe/Ag	> 10 layers	No	[9]
0	$5 \cdot 10^6$	~ few 10	Ag/Au	9-15 layers	No	[10]
10^9	10^{11}	-	Ag/Ag	1.5 nm	No	[11]
0	$5 \cdot 10^5$	~ several 10	Ag/Pt, Pt/Pt	1.5 nm	No, Yes	[11]
10^2	$5 \cdot 10^4$	~ 300	Ti/Cu	1.8 nm	Yes	[12]
0	10^5	~ few 10	Ag/Au	15-18 layers	No	[13]

0	10^4	-	Au/Ni, Ni/Ni, Pt/Ni	1 layer	No (common BE)	[14]
10^5	10^8	100	Pt/Ag, Pt/Gr/Ag	1 layer	No	[15]
10^3	**10^7**	**588**	**Ni/Ni**	**5 ± 1 nm**	**Yes**	**This work**

Table S6: Benchmarking table of publications showing TRS in h-BN-based resistive switching devices. $I_{cc,max}/I_{cc,min}$ denote the current compliance window in which the device shows threshold resistive switching behavior. A CMOS-compatible configuration includes a CMOS compatible material stack as well as an application-near device structure like cross point devices. Devices with a common bottom electrode or conductive atomic force microscopy (C-AFM) investigations are considered as not CMOS compatible configurations.

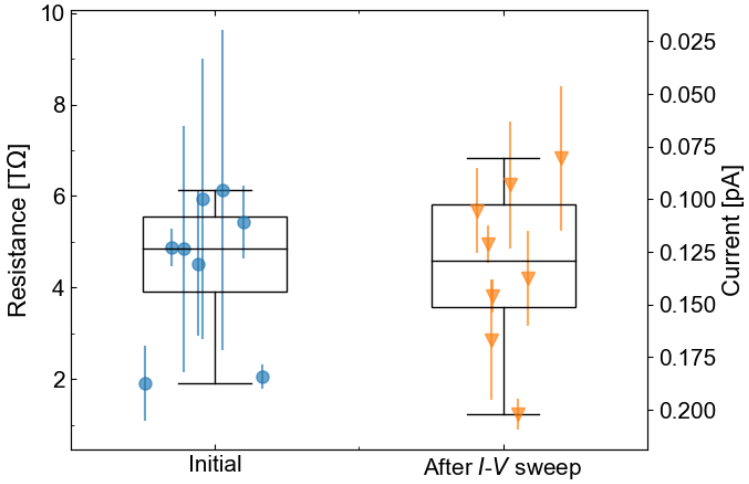

Figure S6: Boxplots of resistances and current levels for 8 different devices. "Initial" represent measurements before any volatile RS events and "After *I-V* sweep" is after performing a RS measurement showing that resistance levels return to the original state. The single measurement points are plotted in the background of each boxplot. The resistance was measured at a voltage of 0.1 V. 15 measurement points were recorded per measurement. The measured current level after the *I-V* sweep serves as the off current for the calculation of the maximum On/Off ratio in table S6.

Section S7: Temperature dependent *I-V* curves of Device in HRS

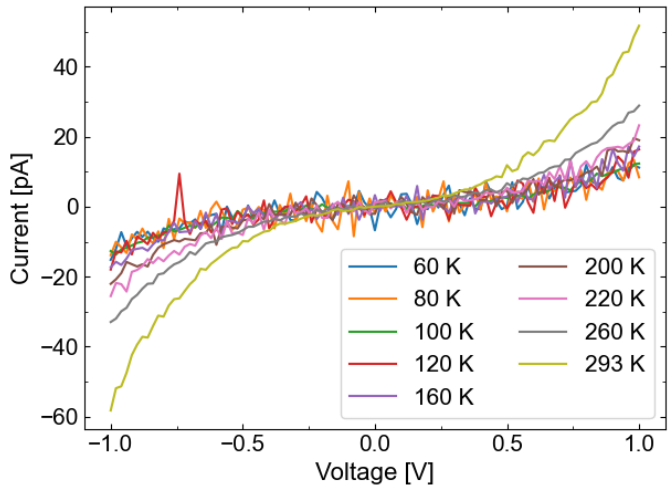

Figure S7: Unfiltered *I-V* data of the temperature dependent measurements of a Ni/h-BN/Ni device in HRS. The *I-V* curves shown in the main paper are smoothened with a Savitzky-Golay filter[16].

Section S8: Algorithm to get the most linear region of a curve according to R²-criterion

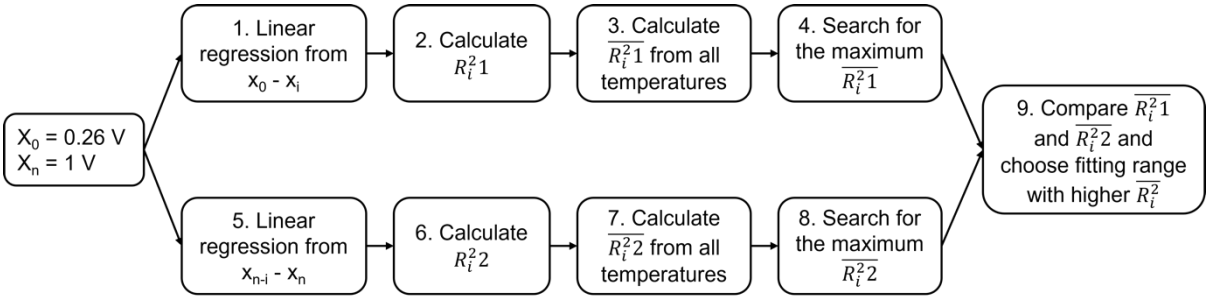

Figure S8: Flow-chart of algorithm to get the most linear region in our *I-V* curve.

The R^2-value is defined as the ratio of the squared deviation of the fitted values from the measured values and the squared deviation of the measured values from the global mean of a linear regression model, and normalized to an absolute value between 0 and 1[17,18]. A value close to 1 denotes a good match of the linear fit to the data, whereas a value close to 0 denotes a bad match of the linear fit to the data.

We exclude the voltage range between 0 V and 0.26 V from our fits because in Figure 3c in the main paper one can see that at a voltage of 0.26 V the measurement noise is high, which will lead to inconsistent results. This means for the fitting algorithm that the minimum fitting range is fixed to x_0 = 0.26 V or its corresponding x-value of the linearized *I-V* data corresponding to the conduction mechanism formula. The following steps are performed to find the most linear region in our curves according to the R²-criterion with the constraint that either the maximum or the minimum of the fitting range is fixed:

1. Perform a linear regression from x_0 to x_i for each temperature, where x_i is the i-th data point and its range is $i = \{10, 11, 12, \dots, n-1, n\}$, where n is the total number of data points.
2. Calculate $R_i^2 1$ for each linear regression. With $i \geq 10$ the smallest linear regression includes 10 data points.
3. Calculate $\overline{R_i^2 1}$, the mean $R_i^2 1$ from all temperatures.
4. Search for the maximum $\overline{R_i^2 1}$.
5. Perform a linear regression from x_{n-i} to x_n, with $i = \{10, 11, 12, \dots, n-1, n\}$.
6. Calculate $R_i^2 2$ for each linear regression.
7. Calculate $\overline{R_i^2 2}$, the mean $R_i^2 2$ from all temperatures.
8. Search for the maximum $\overline{R_i^2 2}$.
9. Compare $\overline{R_i^2 1}$ and $\overline{R_i^2 2}$ and choose the fitting range with the higher $\overline{R_i^2}$.

The fitting range with the highest $\overline{R_i^2}$ corresponds, according to the R^2-criterion, to the most linear region in the curves. The algorithm is summarized in Figure S8.

Section S9: Discussion of various current conduction mechanisms

In this section we discuss the applicability of the Poole Frenkel model, the space charge limited conduction (SCLC) model, the nearest neighbor hopping (NNH) and the Mott variable range hopping (VRH) model to our temperature dependent *I-V* data in the HRS.

The Poole Frenkel CCM assumes that electrons are thermally emitted from traps into the conduction band of the dielectric material and it has a characteristic electric field and temperature dependence of[19]

$$J \sim E \cdot \left[\frac{-q\left(\Phi_T - \sqrt{\frac{qE}{\pi\epsilon_r\epsilon_0}}\right)}{k_B T}\right], \qquad \text{(s1)}$$

where E is the electric field, q is the elementary charge, Φ_t is the trap depth, ϵ_r is the dielectric constant, ϵ_0 is the vacuum permittivity, and k_B is the Boltzmann constant. Considering equation (s1), a plot of $\ln(J/E)$ vs. $\sqrt{E}$ should be linear. The electric field is calculated by dividing the applied voltage by the h-BN film thickness extracted from the HRTEM image in Figure 1f in the main paper. The Poole-Frenkel plot is shown in Figure S9-1. We found the most linear region in the Poole-Frenkel plot between 0.56 V and 1 V. According to equation (s1), we can calculate the dielectric constant of our h-BN film with the slope extracted by the linear regression. The calculated dielectric constants for all temperatures can be found in Table S9-1. We see that the dielectric constant highly depends on the temperature and additionally

has values more than 50 times higher than the literature value of ϵ_r = 5[20]. Thus, we exclude the Poole Frenkel CCM as the responsible CCM in our devices.

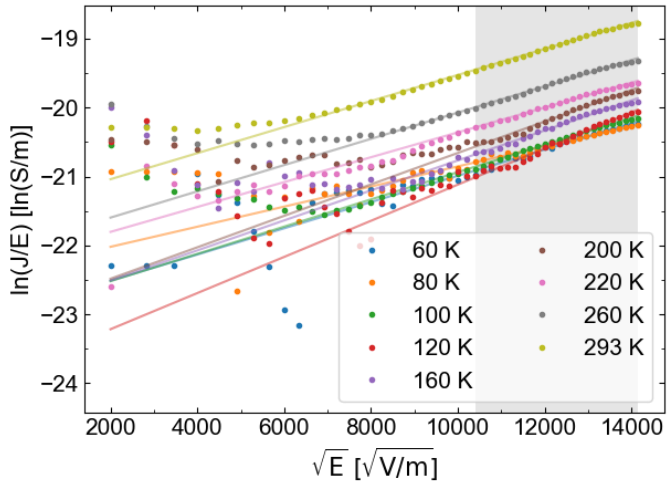

Figure S9-1: Poole-Frenkel plot for all temperatures. The data points with a gray background (10392 $\sqrt{V/m}$ - 14142 $\sqrt{\mathrm{V/m}}$, which corresponds to 0.54 V – 1 V) fit best to a linear model. The lines are the corresponding linear fits.

Temperature [K]	**Dielectric constant ϵ_r**
60	6281
80	5644
100	2047
120	769
160	626
200	357
220	489
260	319
293	253

Table S9-1: Extracted dielectric constants for all temperatures.

The SCLC theory predicts the current density between two plane, parallel electrodes to be split in three regimes, the ohmic conduction current (J_{Ohm}~V), the trap-filled limit current (J_{TFL}~V^2) and Child's law (J_{Child}~V^2), where the current densities depend on the applied voltage as follows:[21]

$$J_{Ohm} = qn_0\mu\frac{V}{d}, \tag{s2}$$

$$J_{TFL} = \frac{9}{8}\mu\epsilon_r\epsilon_0\Theta_0\frac{V^2}{d^3}, \tag{s3}$$

$$J_{Child} = \frac{9}{8}\mu\epsilon_r\epsilon_0\frac{V^2}{d^3}. \tag{s4}$$

n_0 is the concentration of the free charge carriers in thermal equilibrium, μ is the charge carrier mobility, Θ_0 is the ratio of the effective density of states in the conduction band and the density

of traps inside the h-BN, d is the distance between the electrodes, and V is the applied voltage. Between J_{TFL} and J_{Child} is a transition region where $J \sim V^x$ with $x > 2$. We expect to be only in the first two regions, as we apply relatively low voltages. For this CCM we do not apply our algorithm for maximized R^2-value but adapt it to find the fitting range leading to a slope of 2 (with a fixed maximum of the fitting range at 1 V) and the fitting range leading to a slope of 1 (with a fixed minimum of the fitting range at the second data point at 0.06 V). This procedure leads to an overlap of the fitting ranges, so we adjust the overlap region manually in a way that there is no overlap and at the same time the R^2 values remain close to 1. In Table 9-2 the extracted slopes of the linear regression fits can be found. With the equations (s2) and (s3) one can extract the mobility of the charge carriers from the intercept of the fitted lines. However, in the case of the ohmic conduction region, we must estimate n_0 to calculate the mobility, and in the case of the TFL region, we must estimate θ. We will only extract the mean mobility from all temperatures as we must estimate the values for θ and n_0 anyways, which is a relatively big error source. A. Rose[22] gives an approximate value for θ of $\sim 10^{-7}$. With this, we estimate the mean mobility in the TFL region of all temperatures to be $\mu_{mean} = (1.42 \pm 0.88) \cdot 10^{-4} \frac{cm^2}{Vs}$, which is comparable to the values extracted by Chiu et. al.[23,24] for other insulators. However, the extraction of a realistic value for the mobility in the ohmic region is not possible. We found no applicable literature value for n_0. To get a first estimation of the mobility we set n_0 to 1. This results in a mean mobility of $\mu_{mean} \approx 5 \cdot 10^{13} \frac{cm^2}{Vs}$. This means, n_0 must be in the order of $10^{17} \frac{1}{cm^3}$ to get a comparable value for the mobility in both regions, which is unrealistic for a wide-bandgap, insulating material like h-BN at low temperatures (< 260 K).

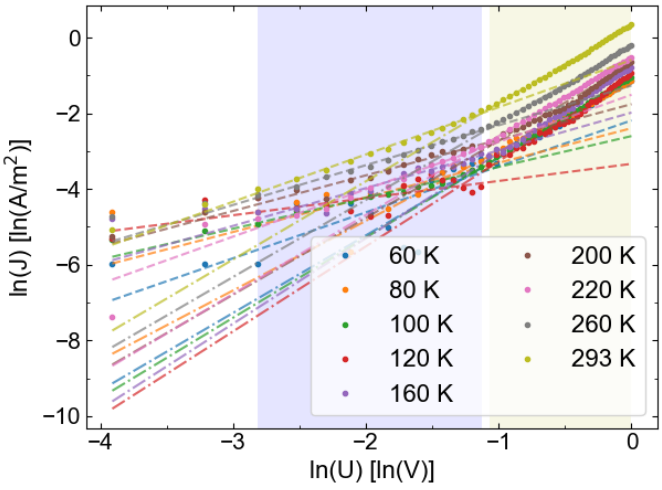

Figure S9-2: Characteristic space charge limited CCM plot for all temperatures. The blue and yellow regions mark the fitting range for ohmic conduction regime and trap-filled limit current

regime, respectively. The dashed and dash-dotted lines are the fits of the blue and yellow region, respectively.

T [K]	Slope blue region	R^2 blue region	Slope yellow region	R^2 yellow region
60	1.21	0.448	2.05	0.993
80	0.91	0.526	1.84	0.994
100	0.81	0.975	2.12	0.999
120	0.45	0.368	2.24	0.985
160	1.00	0.916	2.25	0.996
200	0.94	0.940	2.03	0.987
220	1.24	0.979	2.08	0.999
260	1.05	0.995	2.03	0.998
293	1.25	0.994	2.06	0.999

Table 9-2: Extracted slopes of linear regression fits for different temperatures in respective regions of the characteristic SCLC plot.

The NNH and Mott VRH mechanisms assume electrons hopping through the dielectric from traps to traps via nearest neighboring traps with a certain barrier height, or traps with a variable (wider) distance but possibly a lower energy barrier, respectively. The models describe a characteristic temperature dependence of[25]

$$\sigma = \sigma_0 \cdot e^{-(T_0/T)^{\beta}}, \tag{s5}$$

where σ is the conductance, σ_0 is the conductivity at a certain temperature T_0, T is the temperature, and β is a parameter dependent on the model under consideration. In the NNH and Mott VRH models $\beta = 1$ and $\beta = \frac{1}{4}$, respectively. In contrast to the CCMs discussed before we need to measure the temperature dependent conductance of our devices to apply these models. This is done by calculating the inverse of the resistance shown in Figure 3b in the main paper, which was measured at a voltage of 0.1 V. By extracting T_0 one can calculate the hopping energy[26]

$$E_h(T) = \frac{1}{4} k_b T^{3/4} T_0^{1/4}, \tag{s6}$$

which reflects the energy barrier between defects. From equation (s5), one expects a linear behavior when the natural logarithm of the conductance is plotted over $\frac{1}{T^{\beta}}$. The characteristic plots for NNH and Mott VRH are shown in Figures S9-3 and S9-4, respectively. Both plots exhibit a nonlinear behavior over the full temperature range, but a linear region for temperatures

≥ 160 K can be identified in both plots. In the smaller temperature range the data points seem to be linear, too. However, having a closer look to the fit statistics let us exclude these temperatures from our further analysis due to the high noise in the measurement (compare argumentation to the Arrhenius plot discussed in the main paper). According to equation (s5), T_0 depends on the slope of the linear fit and σ_0 is related to the intercept of the linear fit. Conducting a linear fit for temperatures ≥ 160 K in the NNH plot we get T_0 = -564 K and σ_0 = 44 pS. The negative T_0 would lead to a negative hopping energy, which is physically not meaningful. Thus, we exclude NNH as a possible conduction mechanism.

We find $T_0 = 23.31 \cdot 10^5$ K and σ_0 = 84 nS by fitting the region for $T \geq 120$ K in the Mott VRH characteristic plot. According to equation (s6), we get a mean $E_h = 49 \pm 8$ meV.

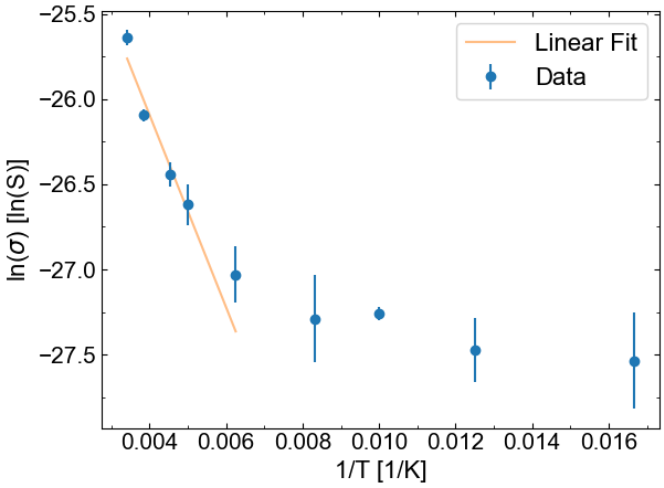

Figure S9-3: Nearest neighbor hopping plot.

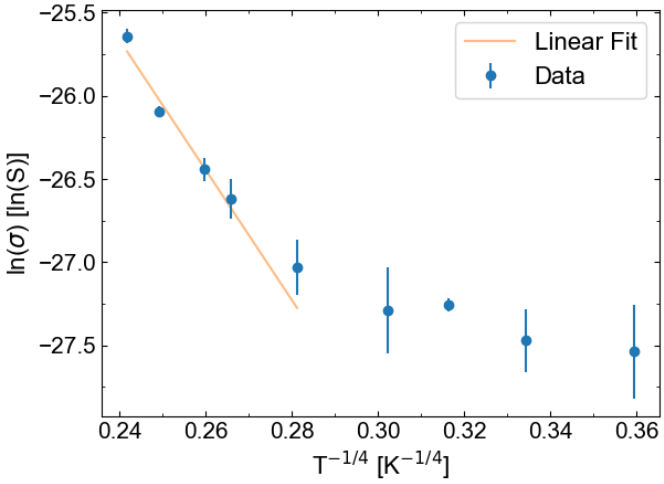

Figure S9-4: Mott variable range hopping plot.

Section S10: Hopping conduction

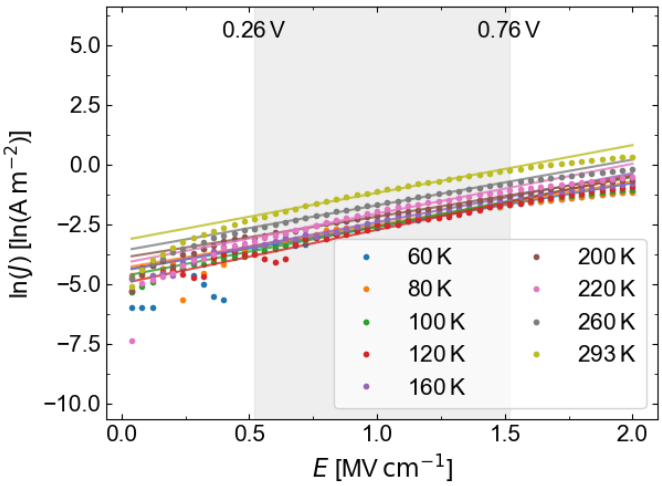

Figure S10: Characteristic hopping conduction plot without an additional offset.

Section S11: Trap assisted tunneling

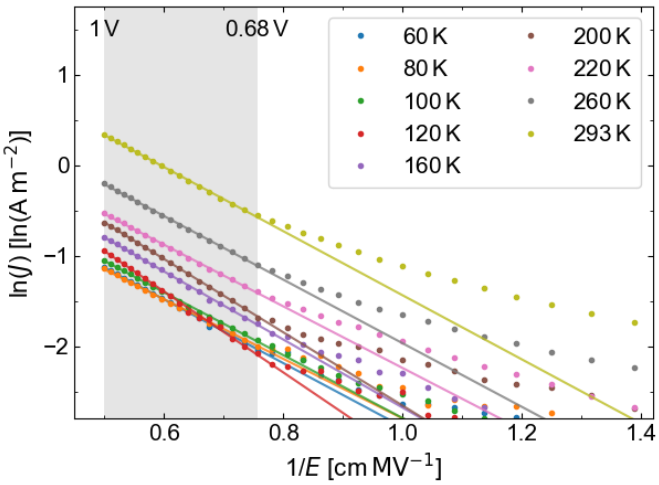

Figure S11: Characteristic trap assisted tunneling plot without an additional offset.

Section S12: Temperature dependent I-V measurements of a device in permanent LRS

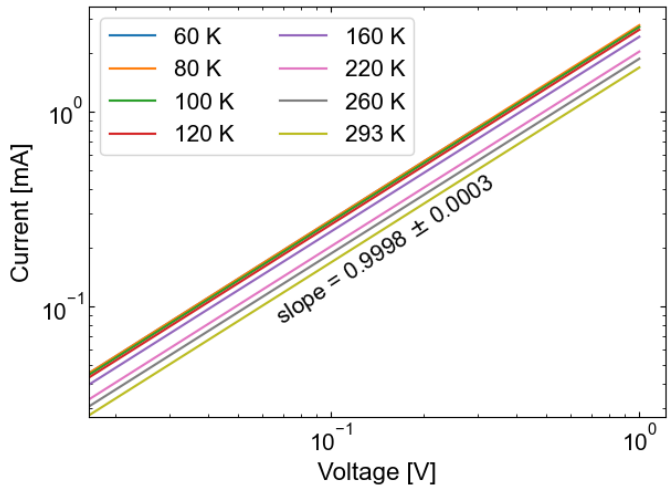

Figure S12: Double-logarithmic plot of I-V curves shown in Figure 4a in the main paper. All curves show clear linear behavior with a mean slope of 0.9998 ± 0.0003 A/V.

Section S13: Energy filtered TEM (EFTEM) images

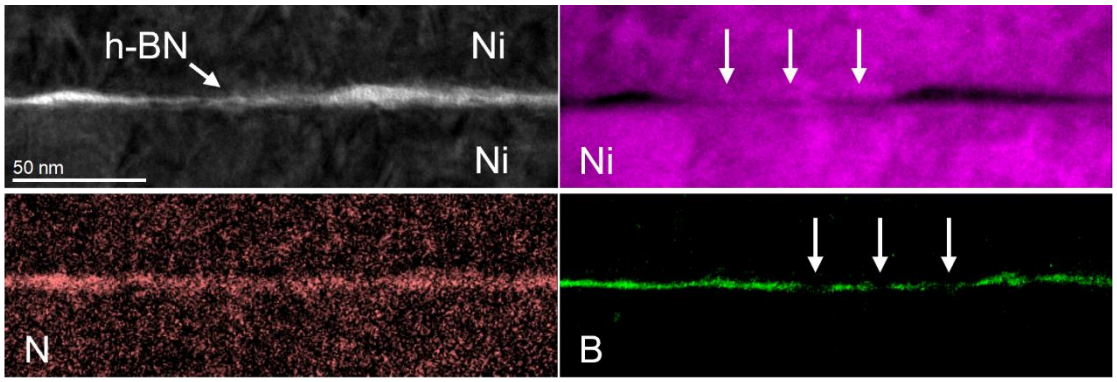

Figure S13: Cross-section TEM and EFTEM images of nickel, nitrogen, and boron.
Due to drift of the TEM-lamella between the different EFTEM measurements the marked features do not appear at the same positions. However, referencing the EFTEM maps to the cross-section TEM image let us create the overlay-image shown in Figure 4d in the main paper. The nitrogen map reveals no distinct defects in the h-BN film.

Section S14: Alternative filter method of temperature-dependent *I-V* curves of a device in HRS and corresponding analysis

Below we performed the analysis described in our manuscript but with a moving average filter applied to our measured *I-V* data. The resulting physical parameters remain, within the error margins, the same, which shows that our method is robust against different filter methods.

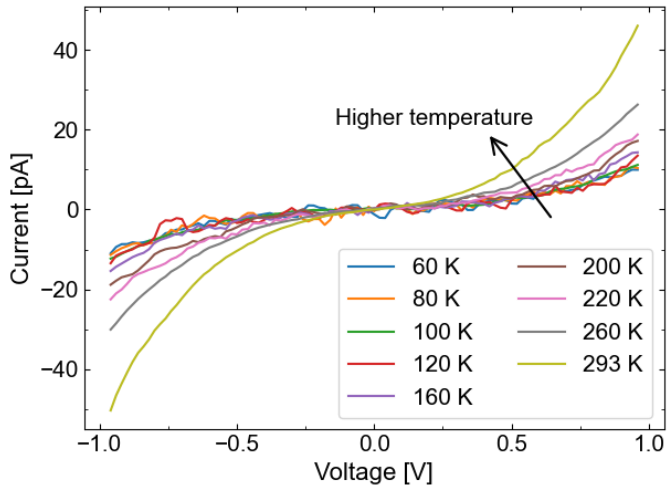

Figure S14-1: *I-V* curves of Figure S7 filtered with a moving average filter (average window size is 5 data points). Please note that the data is only plotted between -0.96 V and 0.96 V because the moving average filter cuts of data points at the edge of the measurement array.

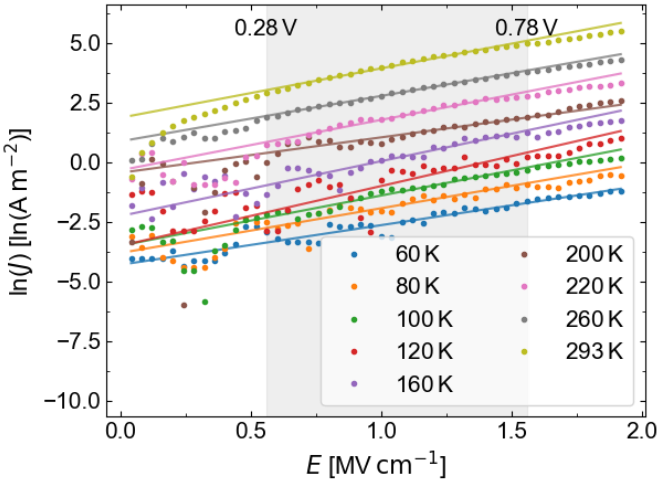

Figure S14-2: Hopping conduction plot of the *I-V* data in Figure S14-1. Our algorithm gives us the most linear region of our data in the voltage range between 0.28 V and 0.78 V with a mean R^2-value of 0.94. We get a hopping distance of a = 2.9 ± 1.4 Å and a trap depth of Φ = 80 ± 22 meV. All the extracted values are, within the scope of their errors, the same as in the manuscript.

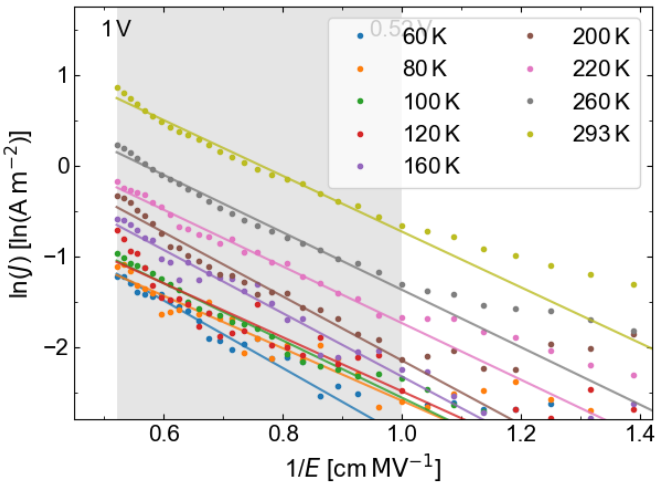

Figure S14-3: Trap assisted tunneling plot of the *I-V* data in Figure S14-1. Our algorithm gives us the most linear region of our data in the voltage range between 0.52 V and 0.96 V. This is a noticable difference to the analysis in the manuscirpt, where we get the most linear region between 0.68 V and 1 V. However, the trap energy level is calculated to Φ = 0.10 ± 0.01 eV, which is, within its error margins, the same as the trap energy level which we get in our manuscipt.

Section S15: Analysis of temperature-dependent *I-V* curves of a device in HRS without filtering

Below we performed the analysis shown in the manuscript but with no filter applied to our measurement *I-V* data (compare Figure S7). Because outliers now have a strong weight on the automatic finding of the most linear region in our data, we cannot apply our automated R²-method to the data anymore. However, we used the fitting ranges found by the algorithm on our Savitzky-Golay-filtered data and discuss the extracted physical parameters here. The resulting physical parameters remain, within the error margins, the same.

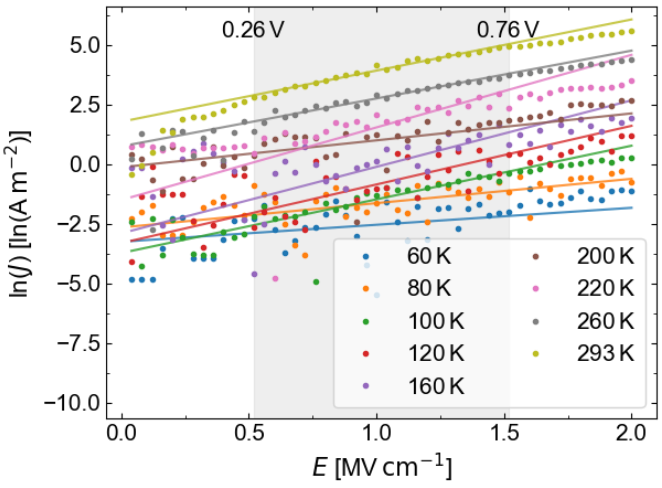

Figure S15-1: Hopping conduction plot of the unfiltered *I-V* data. When we fit the data in the voltage region we found with the filtered data, we get a hopping distance of a = 3.00 ± 1.98 Å and a trap depth of Φ = 79 ± 30 meV. In the low temperature regime the variation of the slopes is high, which is reflected in a higher error of the extracted values. Nevertheless, the values fit to the ones extracted in the manuscript. Note that the noise is reduced for temperatures ≥ 260 K, which is reflected in a good R^2 value of ~0.97 for the fits of the *I-V* curves measured at this temperatures.

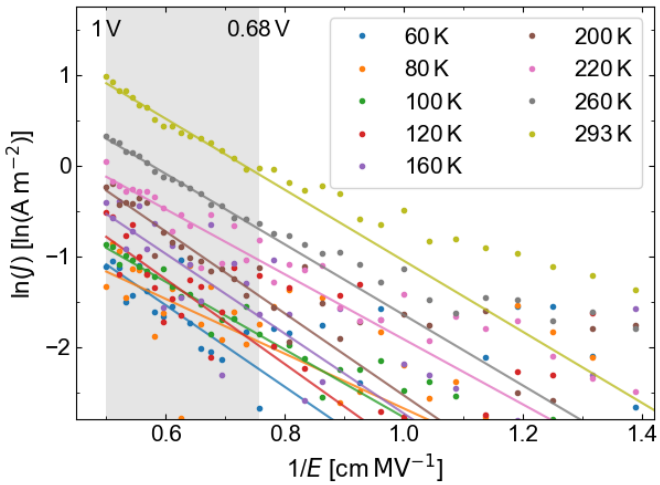

Figure S15-2: Trap assisted tunneling plot of the unfiltered *I-V* data. We get a trap energy level of Φ = 0.12 ± 0.02 eV when fitting it in the voltage range we used in the manuscript. Here, the same argumentation holds as for Figure R5: The data points in the lower temperature regime display higher variation due to the noise, but for temperatures ≥ 260 K less noise leads to reasonable good R^2 values of ~0.98 even without filtering.

References

[1] L. H. Li, J. Cervenka, K. Watanabe, T. Taniguchi, Y. Chen, *ACS Nano* **2014**, *8*, 1457.

[2] J. Wang, F. Ma, M. Sun, *RSC Adv.* **2017**, *7*, 16801.

[3] L. H. Li, E. J. G. Santos, T. Xing, E. Cappelluti, R. Roldán, Y. Chen, K. Watanabe, T. Taniguchi, *Nano Lett.* **2015**, *15*, 218.

[4] A. Ranjan, N. Raghavan, S. J. O'Shea, S. Mei, M. Bosman, K. Shubhakar, K. L. Pey, *Sci. Rep.* **2018**, *8*, 1.

[5] G. Dastgeer, H. Abbas, D. Y. Kim, J. Eom, C. Choi, *Phys. Status Solidi RRL – Rapid Res. Lett.* **2020**, *15*, 2000473.

[6] R. D. Nikam, K. G. Rajput, H. Hwang, *Small* **2021**, *17*, 2006760.

[7] C. Pan, Y. Ji, N. Xiao, F. Hui, K. Tang, Y. Guo, X. Xie, F. M. Puglisi, L. Larcher, E. Miranda, L. Jiang, Y. Shi, I. Valov, P. C. McIntyre, R. Waser, M. Lanza, *Adv. Funct. Mater.* **2017**, *27*, 1604811.

[8] F. Hui, M. A. Villena, W. Fang, A.-Y. Lu, J. Kong, Y. Shi, X. Jing, K. Zhu, M. Lanza, *2D Mater.* **2018**, *5*, 031011.

[9] M. A. Villena, F. Hui, X. Liang, Y. Shi, B. Yuan, X. Jing, K. Zhu, S. Chen, M. Lanza, *Microelectron. Reliab.* **2019**, *102*, 113410.

[10] B. Yuan, X. Liang, L. Zhong, Y. Shi, F. Palumbo, S. Chen, F. Hui, X. Jing, M. A. Villena, L. Jiang, M. Lanza, *Adv. Electron. Mater.* **2020**, *6*, 1900115.

[11] S. Chen, M. R. Mahmoodi, Y. Shi, C. Mahata, B. Yuan, X. Liang, C. Wen, F. Hui, D. Akinwande, D. B. Strukov, M. Lanza, *Nat. Electron.* **2020**, *3*, 638.

[12] Y. Shi, C. Pan, V. Chen, N. Raghavan, K. L. Pey, F. M. Puglisi, E. Pop, H.-P. Wong, M. Lanza, In *2017 IEEE International Electron Devices Meeting (IEDM)*, **2017**, p. 5.4.1-5.4.4.

[13] Y. Shi, X. Liang, B. Yuan, V. Chen, H. Li, F. Hui, Z. Yu, F. Yuan, E. Pop, H.-S. P. Wong, M. Lanza, *Nat. Electron.* **2018**, *1*, 458.

[14] Y. Li, Z. Cui, Y. He, H. Tian, T. Yang, C. Shou, J. Liu, *Appl. Phys. Lett.* **2022**, *120*, 173104.

[15] R. D. Nikam, H. Hwang, *Adv. Funct. Mater.* **2022**, *32*, 2201749.

[16] Abraham. Savitzky, M. J. E. Golay, *Anal. Chem.* **1964**, *36*, 1627.

[17] N. R. Draper, H. Smith, *Applied regression analysis*, 3rd ed., Wiley, New York, **1998**.

[18] J. L. Devore, *Probability and statistics for engineering and the sciences*, Eighth edition., Brooks/Cole, Cengage Learning, Boston, MA, **2012**.

[19] E. W. Lim, R. Ismail, *Electronics* **2015**, *4*, 586.

[20] Y. Y. Illarionov, T. Knobloch, M. Jech, M. Lanza, D. Akinwande, M. I. Vexler, T. Mueller, M. C. Lemme, G. Fiori, F. Schwierz, T. Grasser, *Nat. Commun.* **2020**, *11*, 1.

[21] F.-C. Chiu, S. Mondal, T.-M. Pan, In *High-k Gate Dielectrics for CMOS Technology*, John Wiley & Sons, Ltd, **2012**, pp. 111–184.

[22] A. Rose, *Phys. Rev.* **1955**, *97*, 1538.

[23] F.-C. Chiu, C.-Y. Lee, T.-M. Pan, *J. Appl. Phys.* **2009**, *105*, 074103.

[24] F.-C. Chiu, *J. Appl. Phys.* **2007**, *102*, 044116.

[25] N. F. Mott, E. A. Davis, *Electronic Processes in Non-Crystalline Materials*, Oxford University Press, Oxford, New York, **2012**.

[26] S. Ravi, M. Kar, *Phys. B Condens. Matter* **2004**, *348*, 169.